Research Article Vol. 2, No. 6 / 15 June 2019 / OSA Continuum 2065

Heterogeneous integration of $KY(WO_4)_2$-on-glass: a bonding study

CARLIJN I. VAN EMMERIK,[1,*] RAIMOND FRENTROP,[1] MEINDERT DIJKSTRA,[1] FRANS SEGERINK,[1] ROY KOOIJMAN,[2,3] MUHAMMAD MUNEEB,[4] GUNTHER ROELKENS,[4] ELISE GHIBAUDO,[5] JEAN-EMMANUEL BROQUIN,[5] AND SONIA M. GARCIA-BLANCO[1]

[1] *Optical Sciences, MESA+ Institute for Nanotechnology, University of Twente, 7500 AE Enschede, The Netherlands*
[2] *Techno Centrum voor Onderwijs en Onderzoek, Glas instrumentmakerij, University of Twente, Drienerlolaan 5, 7522 NB, Enschede, The Netherlands*
[3] *Currently at PHIX, De Veldmaat 17, 7522 NM Enschede, The Netherlands*
[4] *Photonics Research Group, INTEC Department, Ghent University-imec, Technologiepark-Zwijnaarde, Ghent 9052, Belgium*
[5] *Univ. Grenoble Alpes, Univ. Savoie Mont Blanc, CNRS, Grenoble INO, IMEP-LAHC, 38000 Grenoble, France*
[*] *c.i.vanemmerik@utwente.nl*

Abstract: Rare-earth ion doped potassium yttrium double tungstate, RE:$KY(WO_4)_2$, is a promising candidate for small, power-efficient, on-chip lasers and amplifiers. There are two major bottlenecks that complicate the realization of such devices. Firstly, the anisotropic thermal expansion coefficient of $KY(WO_4)_2$ makes it challenging to integrate the crystal on glass substrates. Secondly, the crystal layer has to be, for example, <1 μm to obtain single mode, high refractive index contrast waveguides operating at 1550 nm. In this work, different adhesives and bonding techniques in combination with several types of glass substrates are investigated. An optimal bonding process will enable further processing towards the manufacturing of integrated active optical $KY(WO_4)_2$ devices.

1. Introduction

Potassium yttrium double tungstate ($KY(WO_4)_2$) is a promising candidate for on-chip lasers and amplifiers. Its relatively high refractive index ($n \approx 2$ at 1550 nm [1,2]) makes it suitable for the fabrication of devices with a small footprint. The crystal provides large emission and absorption cross-sections for rare-earth ions doped into the material [3]. Furthermore, large concentrations of rare-earth ions can be introduced into the crystal matrix without undesirable quenching effects, thanks to the long interionic distances between the atoms ($\langle d \rangle \approx 0.4$ nm [4]).

Its crystalline structure is also advantageous to achieve excellent gain characteristics when doped with rare-earth ions, which is needed for the realization of lasers and amplifiers. However, the integration of $KY(WO_4)_2$ on glass substrates is challenging. Firstly, $KY(WO_4)_2$ has to be grown on a lattice matched substrate, i.e., growth of slightly doped $KY(WO_4)_2$ on an undoped $KY(WO_4)_2$ seed substrate by liquid phase epitaxy (LPE) [5,6], which makes this method not suitable for the integration of the material on amorphous substrates. Secondly, the $KY(WO_4)_2$ sample has a large (~250-650%) thermal expansion coefficient (CTE) mismatch with the glass substrate, which gives restrictions on the thermal budget that can be used during the integration process.

Previous studies have demonstrated waveguide lasers with high efficiency and high output power at a wavelength of 2 μm [7] and lasers at ~1 μm wavelength with large tuning bandwidth [8,9], fabricated using LPE [6]. Those devices have a comparable performances as waveguide

#365430 https://doi.org/10.1364/OSAC.2.002065
Journal © 2019 Received 1 May 2019; revised 29 May 2019; accepted 29 May 2019; published 13 Jun 2019

OSA CONTINUUM

lasers made by laser writing in various glasses (i.e., ZBLAN [10], bismuthate glass [11]) and crystals (i.e., $GdVO_4$ [12], YAG [13,14]) but with lower lasing threshold. Both fabrication methods result in relatively large structures due to the low refractive index contrast between core and cladding (i.e., $\Delta n \sim 0.02$ [6] with LPE, $\Delta n \sim 0.003$ [15] with laser writing). High refractive index contrast rib $KY(WO_4)_2$ waveguides have been demonstrated by Sefünç et al [16], where a bulk crystal of 10×10 mm^2 and 1 mm thickness has been bonded with a UV-curable optical adhesive to a SiO_2 substrate and thinned to ~2.4 µm. Optical waveguides were patterned using focused ion beam (FIB) milling. This method is, however, not suitable for the realization of long devices (i.e., several millimeters) and it doesn't allow for scalability. Therefore, we aim at a comparable integration method where the devices can be made with standard UV-lithography and reactive ion etching to enable scalability.

There are a few requirements that have to be met for the fabrication of optical $KY(WO_4)_2$-on-glass devices. Firstly, the bond has to be free of defects at the interface between the $KY(WO_4)_2$ sample and the glass substrate because interfacial defects increase scattering losses, which harms the performance of optical devices. Defects at the interface can also induce cracking of the samples in the later thinning and polishing step. Secondly, the bond needs to have a high strength to survive the thinning procedure. Additionally, the bond line should be uniform within tens of nanometers such that the optical devices patterned on the surface of the chip have similar thickness and therefore similar performance. Finally, the materials used for the integration should be CMOS compatible for future integration with passive platforms (such as Si or Si_3N_4).

This paper focusses on the integration method of a bulk $KY(WO_4)_2$ crystal onto a glass substrate. Different bonding methods, in combination with various adhesives, are tested. The advantages and disadvantages of each method are discussed to satisfy the requirements for the fabrication of high refractive index ctrast optical waveguides.

2. Material properties

2.1. $KY(WO_4)_2$ crystal

$KY(WO_4)_2$ is a monolithic, birefringent crystal with three crystalline axes (**a*, -b*, c*** in I2/c space group and **a, b, c** in the C2/c space group), three optical axes ($N_g > N_m > N_p$ [1]) and three CTE tensors ($X_3' > X_1' > X_2'$). The position of the optical axes with respect to both crystal space groups is shown in Fig. 1(a) and the thermal axes are shown in Fig. 1(b). The maximum and minimum of the CTE tensor, X_3' (≈ 21.0 ppm/°C) and X_1'. (≈ 7.2 ppm/°C), are close to the **c*** and **a***-axis, respectively (Fig. 1(b)). The difference in CTE between the crystalline axes does not cause any problem when the crystal is heated while not attached to a substrate. However, bonding of a $KY(WO_4)_2$ crystal at elevated temperatures to, for example, a silicon wafer with a layer of thermal oxide ($CTE_{TEOS} \approx 3.3$ ppm/°C) induces stress in the layers after cooling, which leads to cracks in either the sample or substrate.

2.2. Glass substrates

The CTE anisotropy in $KY(WO_4)_2$ can induce stress/strain when bonded to a glass substrate at elevated (>150 °C) temperatures. The CTE in the **a*-c*** crystalline plane of $KY(WO_4)_2$ is respectively 8.5-19.7 ppm/°C [17].

Two different glass types have been studied to minimize the CTE mismatch between the glass substrate and the **a*-c*** crystalline plane of $KY(WO_4)_2$. MEMpax (SCHOTT AG, MEMpax, DE), a borosilicate glass, has a CTE of 3.3 ppm/°C [18], which corresponds to that of silicon and mimics the thermal oxide grown on a silicon wafer. There is a large CTE mismatch between MEMpax and the two in-plane $KY(WO_4)_2$ axes, which makes it unsuitable for bonding purposes where elevated temperatures are involved. Soda-lime glass has a CTE between 9.1-9.4 ppm/°C

OSA CONTINUUM

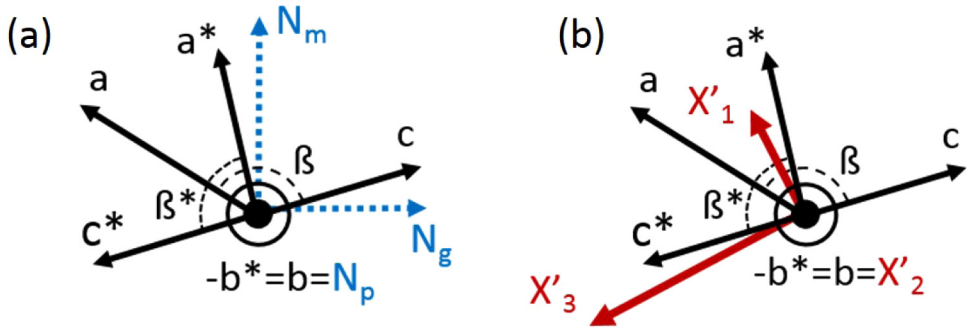

Fig. 1. Crystalline axes (black) with structure according to I2/c space group with **a*** = 1.063 nm, **-b*** = 1.034 nm, **c*** = 0.755 nm**, ß*** = 94.3 ° and **a** = 0.807 nm, **b** = 1.034 nm, **c** = 0.755 nm**, ß** = 130.7 ° from the C2/c space group together with (a) the optical axes (blue); (b) the principle thermal axes (red) [17].

[19,20]. This value is close to that of $KY(WO_4)_2$ and therefore soda-lime substrates are used when elevated temperatures (>150 °C) are required.

2.3. Adhesives

The bonding process and adhesive that are used are important to successfully bond a $KY(WO_4)_2$ sample on a glass substrate. UV-curable adhesives are optimal for room temperature bonding. Bohle low viscosity 740 (Verifix LV 740, Bohle BV) and Norland Optical Adhesive 81 (NOA81, Norland Products Inc.) where selected because of their low viscosity and large strength in comparison to other optical adhesives. Two epoxy based adhesives, Epotek 353ND and 377 (Epoxy Technology Inc.), were selected to test bonding at 150 °C. And finally divinylsiloxane-bis-benzocyclobutene (DVS-BCB, Cyclotene 3022-35, Dow Chemical), referred to as BCB [21,22], and O_2 activated direct bonding [23,24] were selected because of the accuracy in the achievable bond line. A disadvantage of the latter methods is the curing/annealing temperature, which is around 250 °C for an optimal strong bond. The curing/annealing can be performed at lower temperatures (~150 °C), leading to longer process times (>10 hours) and often to weaker bonds [25]. The specifications of the mentioned adhesives are shown in Table 1.

Table 1. Specifications of the different adhesives used.

Adhesive Cure setting → & Properties Name ↓	Cure type	Cure dose	DV at 25 °C (cps)	TS (MPa)	SM (MPa)	CTE <90 °C (ppm/ °C)	$T_{degrade}$ (°C)	n ($\lambda \approx$ 600 nm)	Ref
Bohle LV 740	365 nm	1 J/cm^2	100	–	17.0	–	120	1.50	[26]
NOA 81	365 nm	2 J/cm^2	300	1.4	–	200	125	1.56	[27]
Epotek 353ND	150 °C	1 hour	3000 - 5000	–	>13.8	54	250	1.57	[28]
Epotek 377	150 °C	1 hour	150 - 300	–	10.0	57	300	1.52	[29]
BCB	160 - 250 °C	10 - 1 hours	–	2.9	–	42	350	1.55	[30]
Direct bonding	150 °C	72 h	NaN	–	–	NaN	–	NaN	[25]

DV = dynamic viscosity, TS = tensile strength, SM = shear modulus, $T_{degrade}$ = degradation temperature of the adhesive, n = refractive index

OSA CONTINUUM

3. Bonding methodology

Multiple bonding techniques have been investigated to integrate $KY(WO_4)_2$ samples onto glass substrates. In the following sections, the different bonding techniques are described, namely manual bonding, bonding using a flip-chip bonder and bonding using a wafer bonder instrument.

3.1. Manual bonding

For stability during the thinning process, three $KY(WO_4)_2$-on-glass assemblies need to be mounted on an ultra-parallel glass plate (Ø 83 mm, thickness 6 mm, Logitech, UK) as shown in Fig. 2(a). This imposes stringent requirements on the thickness and uniformity of the different layers in each of the three stacks, namely the glass substrates, the $KY(WO_4)_2$ samples and the adhesive layers in between, since it determines the final uniformity of the thin $KY(WO_4)_2$ slabs.

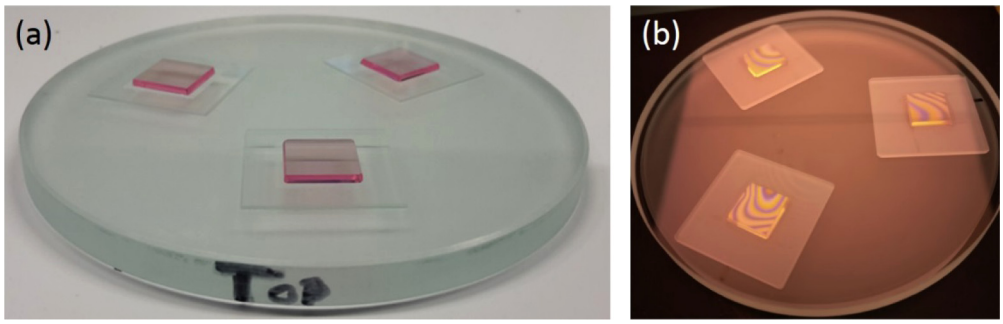

Fig. 2. Photographs of (a) three stacks consisting of $KY(WO_4)_2$ sample bonded with UV-curable adhesive onto MEMpax substrates and wax mounted on an ultra-parallel supporting glass for thinning and polishing. (b) Three stacks consisting of $KY(WO_4)_2$ samples on grinded soda-lime substrates with Newton rings, visible on the $KY(WO_4)_2$-optical flat interface, to check the planarity of the stacks.

The first step in the bonding protocol is to ensure that all the glass substrates have identical thickness. To that aim, both the top and bottom surfaces are grinded on a cast iron disk using a 800 SiC slurry. This step also permits enhancing the adhesion with the substrate. The thickness of the substrates is measured at the center and at the four corners of the substrate with a thickness measurement system equipped with an inductive probe with an accuracy of 0.2 µm (Milimar C1208 and P1300, Mahr, GmbH, DE). If the height at those five points is not within the accuracy of the measurement system (i.e., 0.2 µm), additional grinding is done exerting higher pressure on the areas where the layer is thicker than the rest of the substrates. This process is repeated until all samples are parallel and have identical thickness (i.e., ± 0.4 µm due to repeatability, hysteresis and error limit of the measurement system). With the same measurement technique, three identical $KY(WO_4)_2$ samples (Altechna, LT) are selected from the batch of samples.

In order to verify that the glass substrates and $KY(WO_4)_2$ samples form an identical stack, they are positioned on top of the ultra-parallel plate. An optical flat is then placed on top of this configuration and illuminated with monochromatic light (Kemet, UK, Sodium line λ=598 nm) to inspect the Newton rings on the top layer. The position of the layer stacks is adjusted until less than 10 bright and dark fringes are visible [Fig. 2(b)]. The $KY(WO_4)_2$ samples are then removed and a drop (~10 µL) of low-viscosity UV-curable adhesive is applied on top of the substrate. The $KY(WO_4)_2$ samples are then carefully placed on top in the same position as before. The planarity of the stack is checked by looking at the Newton rings before curing. Finally, the adhesive is cured with the optical flat on top as load (~0.2 N/cm^2).

OSA CONTINUUM

3.2. Bonding using a flip-chip bonder

A flip-chip bonder (Finetech GmbH, Lambda, DE) is used for precision bonding. The bonder has an in-plane alignment accuracy of ± 0.5 µm and it can apply a uniform force ranging from 0.1 till 400.0 N on a sample. The optimal bonding force was found to be between 100 and 150 N to ensure a bond line of ~1 ± 0.5 µm across the whole sample without defects and/or air traps induced by the bonding force [31]. Prior to bonding, both the sample and the substrate are cleaned for 15 minutes in an ultrasonic bath with DI water to remove particles on the surface followed by a chemical cleaning step in a 99% HNO_3 bath for 10 minutes. Subsequently, both substrate and sample were treated with oxygen plasma (50 sccm O_2, 100 W, 5 minutes) to activate the surfaces.

A gimbal tool was utilized in the flip-chip bonder to ensure perfect planarity between the $KY(WO_4)_2$ sample and the substrate. The gimbal was initialized by applying 400 N on a dummy $KY(WO_4)_2$ sample placed on top of a dummy substrate. The real sample and substrate were then mounted on the top and bottom of the bonder, respectively, and a drop of specified adhesive will be applied on the substrate. The $KY(WO_4)_2$ sample will be put in contact with the substrate by lowering the arm tool of the bonder. The bonding force and curing protocols for the bonding are then applied as required.

3.3. Bonding using a flip-chip bonder and a substrate with pre-etched pillars

To control the thickness and uniformity of the bond line, a structure of pillars (Ø 6 µm, spacing 100, 250 or 500 µm, height ~3 µm) was designed in a recessed region of dimensions 12 x12 mm^2 to mimic a micro-bead filled adhesive, with which a planarity determined by the tolerance of the bead diameter can be achieved [32]. The pillar structures are microfabricated in the glass substrate (i.e., MEMpax or soda-lime glass) using standard lithography and fluorine based reactive ion etching [33]. An optical microscope image of a section of the fabricated structures on a MEMpax substrate is shown in Fig. 3(a). Figure 3(b) shows a schematic of a $KY(WO_4)_2$ sample bonded onto a structured substrate. The pillars determine the bonding height and the adhesive in the recessed region creates a strong bond between the substrate and the $KY(WO_4)_2$ sample. A small number of bubbles can be trapped in the adhesive due to the presence of the pillars, which should be minimized by proper surface activation of both the substrate and the sample by oxygen plasma. The pillars were designed so that the optical devices can be placed around the pillars, avoiding changes in the propagation characteristics of the final devices caused by addition of scattering points.

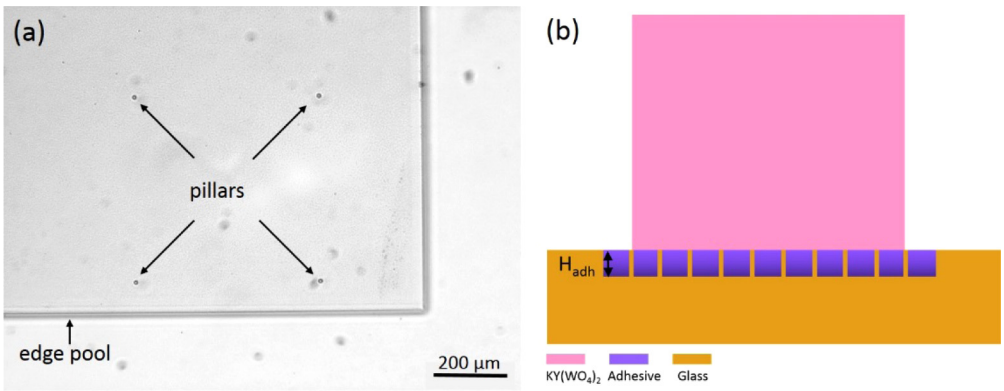

Fig. 3. (a) Top view of an optical microscope image with a corner section of the recessed region (i.e., pool). Inside the recessed region, pillars with a diameter of 6 µm and a spacing of 500 µm are visible. (b) Schematic representation of a $KY(WO_4)_2$ sample bonded on a MEMpax glass substrate with pillars of ~2.8 µm etched in the substrate.

OSA CONTINUUM

3.4. Bonding using a wafer bonder

A wafer bonder, Suss MicroTec ELAN CB6L, was utilized in the bonding tests of $KY(WO_4)_2$ to glass using BCB. Since this instrument is designed for the bonding of full wafers, the sample and substrate were clamped between two Pyrex wafers with a graphite sheet between the sample and the top wafer to equalize the bonding pressure. The temperature and pressure protocols for the bonding are then applied as required.

4. Experimental results

4.1. Bonding using low temperature adhesive

UV-curable adhesives allow bonding at room temperature. Two UV-curable adhesives, Bohle LV740 and NOA81 (Table 1) were investigated in this study.

Manual bonding was utilized to bond $KY(WO_4)_2$ samples onto a 20×20 mm^2 soda-lime substrate using Bohle LV740. The manual bonding process flow described in Section 3.1 was followed. The adhesive was cured with UV-light with a fluence of 1 J/cm^2. The process resulted in a mean bond line of 2.7 µm with ± 1.0 µm variation along the 8 mm length of the sample. A thinner more uniform bond line with a planarity in the tens of nanometer range is required to realize optical devices. To reduce the achievable bond line a larger load is needed. However, a heavier UV-transparent optical flat was not available. Therefore, it is concluded that manual bonding, with the available materials, is not suitable for the envisioned application.

A $KY(WO_4)_2$ sample was bonded onto a 20×20 mm^2 MEMpax substrate using NOA81 and the flip-chip bonder method described in section 3.2. A drop of ~30 µL of NOA81 was applied on the substrate before the sample and substrate where placed in contact. The applied force was built-up with a ramp of 5 N/s until a total force of 100 N was reached. The arm tool stayed down for ~40 seconds. During this time, the adhesive is pre-cured by applying UV-irradiation with a handheld UV-gun (peak wavelength of 365 nm). After bonding, the stack is fully cured with a total dose of 2 J/cm^2 in a UV-oven (Spectrolinker, XL-1500 UV crosslinker). The mean bond line with this procedure was 0.6 µm with a variation of ± 0.4 µm along the 8 mm length of the sample, which is not yet sufficient to fabricate thin $KY(WO_4)_2$ layers with tens of nanometers of maximum variation in thickness.

To increase the bond line uniformity, the method of using a substrate with pre-etched pillars acting as spacers is utilized. Bonding is carried out using NOA81 and the flip-chip bonding procedure onto a MEMpax substrate with microfabricated pillars. The measured bond line was 2.7 µm across the whole sample, which corresponds with the pillar height (i.e., measured height of the pillars was 2.8 ± 0.2 µm). The thickness of the bond line can be accurately controlled by varying the reactive ion etching procedure of the pillars.

4.2. Bonding using high temperature adhesive

Epoxy based adhesives, with curing temperatures of ~150 °C as well as BCB, with curing temperatures ranging from 165-250 °C, were investigated. These adhesives increase the thermal budget in future processes (i.e., $T_{max\_UV} \approx 120$ °C and $T_{max\_epoxy} \approx 250$ °C), such as the deposition of a polishing stop [33] or the integration with a passive photonic platform. Increase of the thermal budget will also ensure a higher reliability during the use and lifetime of the devices. Cracking of the samples occurred due to the combination of the high bonding temperatures and the high CTE mismatch between the sample and the substrate. Trenches oriented along the crystalline direction of lower CTE (i.e., close to the **a***-axis) succeeded in protecting the interface, resulting in a crack and defect free interface, where the optical devices will be fabricated (see section 4.2.3).

OSA CONTINUUM

4.2.1. Bonding using high temperature epoxy

Epoxy based adhesives are typically cured at elevated temperatures (~150 °C) to get maximal bonding strength. To obtain the highest planarity of the bond, a $KY(WO_4)_2$ sample was bonded on a MEMpax substrate with pillars, as described in section 3.3, using a flip-chip bonder.

Prior to bonding, both the substrate and sample had the same cleaning and surface activation process as described in section 3.2. After cleaning and activation, both the sample and substrate were transferred to the flip-chip bonder. Five drops, with a total volume of ~ 30 µL, of Epotek 353ND where placed at the center of the substrate. The curing protocol is as follow: first the temperature is raised to 70 °C for 120 seconds to allow the adhesive to reflow. During the last 30 seconds of this stage, the arm with the sample was lowered and the force was built on the sample with a ramp of 5 N/s up to 150 N where it stayed for 10 minutes. After the reflow step, the temperature was raised to 150 °C for 1 hour to fully cure the adhesive and finally the sample was cooled down to room temperature by natural convection. The first 20 minutes of the curing curve are shown in Fig. 4(a).

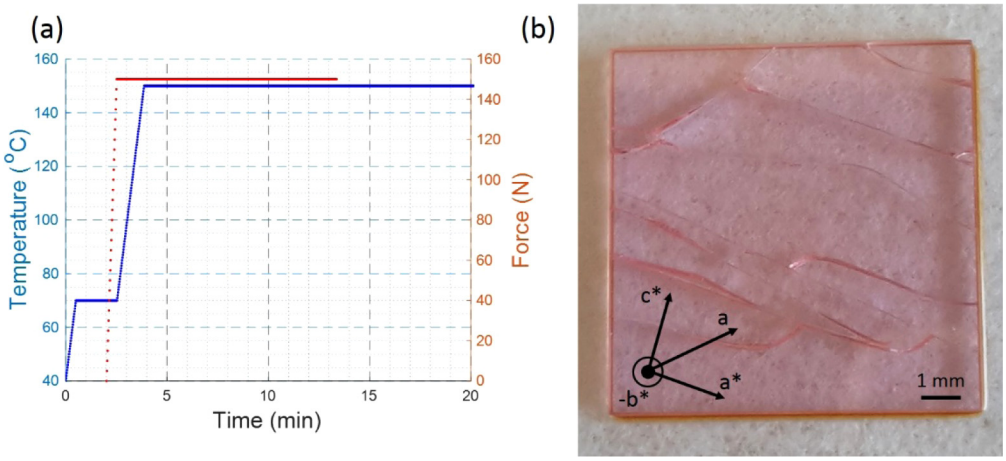

Fig. 4. (a) First 20 minutes of the flip-chip bonding temperature and force profiles. The sample stays at 150 °C for 1 hour before it is cooled by natural convection. (b) Photograph of a $KY(WO_4)_2$ sample bonded on a MEMpax substrate at 150 °C, where cracks mainly occur along the **a***-axis.

The sample cracked during the cooling step when reaching the temperature of 80 °C, which indicates that the stress in the layer was too big due to the CTE mismatch between the $KY(WO_4)_2$ sample and the MEMpax substrate. The cracks are mainly along the **a***-axis, as shown in Fig. 4(b), which can be explained by the fact that the highest thermal expansion is close to the **c***-axis. The **c***-axis is almost perpendicular to the **a***-axis (i.e., angle between **a***-**c*** axis is ~94°), which has the lowest CTE in the **a***-**c*** plane of the crystal. When the crystal cools down, it will be compressed along the **a***-axis and it is most likely to crack in this direction. A few cracks along the **a**-axis of the crystal were also observed. Those cracks cannot directly be explained by the crystalline structure and they are also seen during the growth of lattice and refractive index engineered $KY(WO_4)_2$:Gd, Lu, Yb layers on undoped substrates using liquid phase epitaxy [6].

4.2.2. Bonding using BCB

Benzocyclobutene (BCB) has been reported to provide very uniform, thin, strong bond lines [21], which is ideal for our applications. Therefore, tests were performed to bond a $KY(WO_4)_2$ sample to a soda-lime substrate (to minimize the CTE mismatch) using a 500 nm thick BCB layer. This

OSA CONTINUUM

adhesive is commonly cured at temperatures above 250 °C to obtain the strongest possible bond [30]. In this study, three bonding tests were performed at 230 °C, 190 °C and 165 °C respectively. The corresponding curing times are ~2, 10 and 36 hours, respectively.

Prior to bonding, the sample and substrate were cleaned for 15 minutes in an ultrasonic bath with DI water to remove particles on the surface followed by a chemical cleaning step in a 99% HNO_3 bath for 10 minutes. A mixture of 1:2 = BCB : mesitylene was spincoated at 3000 rpm for 40 seconds on the soda-lime substrate to obtain a 500 nm thick adhesive layer. The sample and substrate are then mounted in the wafer bonder as described in section 3.4. The curing curve is as follows: first, the temperature is raised, with a ramp of ~1.7 °C/min to 150 °C to pre-cure the adhesive for 20 minutes. After pre-curing, the temperature is raised again, with a ramp of ~1.0 °C/min, to the final curing temperature. A bonding force of 165 N is applied on the 4 inch Pyrex wafer during the time of pre-curing and temperature raise. Finally, the sample is cooled by natural convection to roughly 40 °C before unloading. The first part of the bonding procedure is shown in Fig. 5(a). Again, the samples cracked along the **a*-**axis as shown in Fig. 5(b). This indicates that the CTE mismatch between the $KY(WO_4)_2$ sample and soda-lime substrate is still too large.

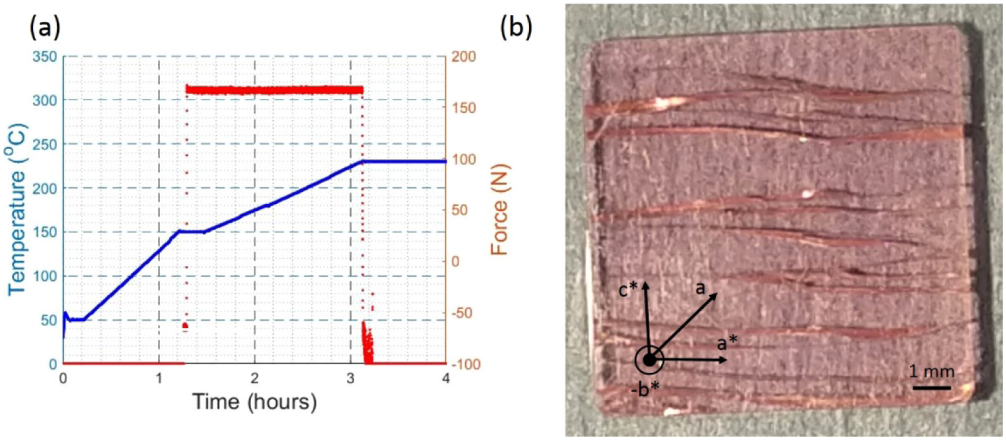

Fig. 5. (a) First 4 hours of bonding temperature and force profile. (b) Photograph of a $KY(WO_4)_2$ sample bonded at 250 °C to a soda-lime substrate, cracks mainly occur along the **a***-axis.

4.2.3. Stress relief trenches in sample

All bonding tests at curing temperatures above 150 °C had cracks mainly along the **a***-axis. In order to bond at elevated temperatures without cracks at the interface between the sample and the substrate, trenches were diced on the surface of the $KY(WO_4)_2$ sample along the **a***-axis to release stress at the interface and guide the cracks to the top surface (i.e., non-bonding surface) of the sample. The trenches are 50 µm wide and 250 µm deep with a heart-to-heart distance of 550 µm along the **a***-axis of the crystal, as can be seen in Fig. 6(a) and (b).

A $KY(WO_4)_2$ sample with trenches was bonded onto a soda-lime substrate (i.e., to have the lowest CTE mismatch between the sample and substrate) using the flip-chip bonder method described in section 3.2. Prior to bonding, the substrate was cleaned for 15 minutes in an ultrasonic bath with DI water to remove particles on the surface followed by a chemical cleaning step in a 99% HNO_3 bath for 10 minutes and functionalized with a 1% saline solution because the oxygen plasma treatment was not sufficient to obtain the correct surface energy match between the substrate and the adhesive. After this step, Epotek 377 was spin-coated at 6000 rpm for 45

OSA CONTINUUM

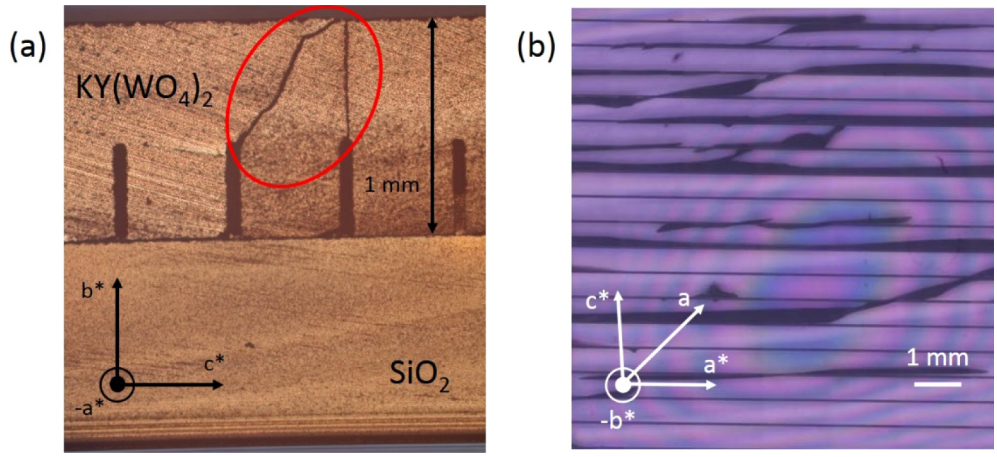

Fig. 6. (a) Side view microscope image of a $KY(WO_4)_2$ sample with trenches bonded with Epotek 377 onto a soda-lime substrate where cracks originate from the top of the trench and propagate towards the top surface of the crystal, indicated with red circle. (b) Photograph in top view of a $KY(WO_4)_2$ sample with trenches bonded with BCB on soda-lime glass. The cracks propagate to the top surface and are mainly along the **a***-axis.

seconds and was reflown at 80 °C for 5 minutes on the heating plate of the flip-chip bonder. After reflow, the $KY(WO_4)_2$ sample was placed in contact with the soda-lime substrate by lowering the arm tool of the flip-chip bonder and the force was built up to 10 N, to prevent that the adhesive bulge up more than 2 µm. The adhesive was finally cured for 1 hour at 150 °C, and afterwards it cooled down by convection.

Again cracks occurred in the layer, as shown in Fig. 6(a), but now they originate from the most inner part of the trench and propagate to the top surface of the crystal. This leaves a defect free interface between the sample and substrate, which potentially can be used for optical devices after the bulk layer is thinned down to the required thickness.

The bonding process with stress relief trenches was repeated using a 1 µm thick BCB layer in the wafer bonder (section 3.4). The process is similar to the one described in section 4.2.2 and the adhesive was cured at 210 °C for 8 hours. In this case the stress was relieved mainly from the trenches (along the **a***-axis) as shown in Fig. 6(b). Some of the cracks propagate in a diagonal from one trench to another along the **a**-axis. As mentioned before, those types of cracks were also reported during the growth of lattice and refractive index engineered $KY(WO_4)_2$:Gd, Lu, Yb layers on undoped $KY(WO_4)_2$ substrates using liquid phase epitaxy [6].

4.3. Direct bonding

A $KY(WO_4)_2$ sample has been bonded onto a custom-made GO14 silicate glass using the direct wafer bonding technique [34]. Direct wafer bonding requires no adhesives and consists of a direct wafer-to-wafer contact between two hydrophilic surfaces. The process induces a surface reorganization based on three mechanisms: spontaneous adhesion based on Van der Walls forces and OH groups, slow fracture effect and consolidation by thermal annealing resulting in the creation of covalent bonds between the two surfaces. Its quality depends on the number of hydroxyl groups at both surfaces and it is therefore strongly dependent upon the cleanness and the activation of the wafers. The process that has been used here is directly derived from the SOI one as described by [34]. The only difference is that the temperature of the thermal annealing has been lowered from above 800°C to 150°C in order to prevent melting of the glass. This change entailed an increase of the annealing time to 72 hours in order to provide enough energy to create

OSA CONTINUUM

the covalent bonds. A previous study [25] showed that, with such a process, a surface energy, γ, greater than 1 J/m^2 is achieved, which allows the bond to withstand standard mechanical processes such as dicing and polishing. After the molecular bonding, both surfaces are crack free, as shown in Fig. 7. With this procedure there is no bond line, which is very promising for future processing and fabrication of optical devices.

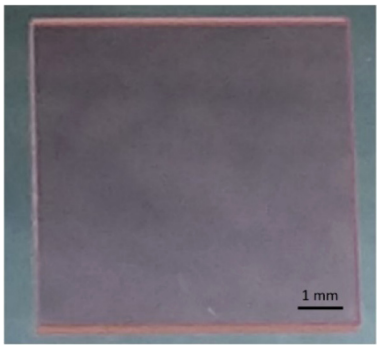

Fig. 7. Photograph of direct bonded $KY(WO_4)_2$ onto GO14 silicate glass.

5. Discussion

In the previous sections, different bonding processes are discussed to integrate $KY(WO_4)_2$ crystals onto glass substrates. Low and high curing temperature adhesives as well as direct bonding have been investigated. All of those methods, together with their associated bonding procedures, have their own advantages and disadvantages.

UV-curable adhesives have as advantage that there is no temperature increase during the bonding process and therefore the CTE mismatch between sample and substrate does not play a role. A substrate mimicking a microbead filled epoxy was developed to fulfill the specifications for the thickness and uniformity of the bond line (i.e., maximum deviation of tens of nanometers across the whole sample). $KY(WO_4)_2$ samples were bonded using a flip-chip bonder with a gimbal tool with UV-curable adhesive (NOA81) to these engineered substrates to achieve a perfectly planar bond across the sample with the desired thickness (i.e., given by the height of the microfabricated pillars in the substrate).

However, in the future integration of the laser crystals to a passive integrated photonics platform, the thermal budget of the adhesive comes into play. The room temperature adhesives used in this study degrade if they are exposed for a long time to a temperature above 120 °C. Therefore high temperature adhesives are studied to increase the thermal budget. However, the high temperature adhesives require curing temperatures above 150 °C. Such high temperatures increase stress due to the large CTE mismatch between the sample and the substrate. Even with a low temperature ramp of <1 °C/min, the sample cracks during cooling. We demonstrate that trenches diced along the **a***-axis of the crystal guide the cracks from the bottom of the trench to the top surface of the sample, leaving a defect free interface between the $KY(WO_4)_2$ sample and the glass substrate. Those trenches, in combination with even smaller BCB bond lines, can pave the way to future integration to other passive platforms.

The most planar bond is achieved using low temperature direct bonding, which is preferential for future integration. This bonding method, however, had the longest annealing time (~72 hours) and need ultra-smooth surfaces (RMS roughness < 1.5 nm [35]). Therefore, additional polishing can be necessary to achieve a void free bonding surface.

OSA CONTINUUM

6. Conclusion

A perfectly planar bond was achieved with a flip-chip bonder using a room temperature curable adhesive and a substrate that mimics a micro bead filled adhesive. For adhesives requiring a curing temperature above 150 °C, cracks appeared upon cooling due to the CTE mismatch between sample and substrate. Stress-relief trenches diced along the **a***-axis made it possible to guide the cracks to the top surface of the crystal. This resulted in a defect-free interface between the crystal sample and glass substrate for the majority of the surface. Finally, a $KY(WO_4)_2$ sample was bonded, for the first time to our knowledge, crack-free to a glass substrate using low temperature direct wafer bonding.

The bonding techniques developed in this work pave the way towards the development of $KY(WO_4)_2$-on-glass devices integrated onto passive technology platforms.

Funding

H2020 European Research Council (ERC) (648978).

Acknowledgments

This project has received funding from the European Research Council (ERC) under the European Union's Horizon 2020 research and innovation program (No. 648978-RENOS).

References

1. A. A. Kaminskii, A. F. Konstantinova, V. P. Orekhova, A. V. Butashin, R. F. Klevtsova, and A. A. Pavlyuk, "Optical and nonlinear laser properties of the $\chi^{(3)}$-active monoclinic α-$KY(WO_4)_2$ crystals," Crystallogr. Rep. **46**(4), 665–672 (2001).
2. X. Mateos, R. Solé, J. Gavaldà, M. Aguiló, J. Massons, and F. Díaz, "Crystal growth, optical and spectroscopic characterisation of monoclinic $KY(WO_4)_2$ co-doped with Er^{3+} and Yb^{3+}," Opt. Mater. (Amsterdam, Neth.) **28**(4), 423–431 (2006).
3. Y.-S. Yong, S. Aravazhi, S. A. Vázquez-Córdova, J. J. Carjaval, F. Díaz, J. L. Herek, S. M. García-Blanco, and M. Pollnau, "Temperature-dependent absorption and emission of potassium double tungstates with high ytterbium content," Opt. Express **24**(23), 26825–26837 (2016).
4. I. M. Krygin, A. D. Prokhorov, V. P. D'yakonov, M. T. Borowiec, and H. Szymczak, "Spin-spin interaction of Dy^{3+} ions in $KY(WO_4)_2$," Phys. Solid State **44**(8), 1587–1596 (2002).
5. W. Bolaños, J. J. Carvajal, X. Mateos, G. S. Murugan, A. Z. Subramanian, J. S. Wilkinson, E. Cantelar, D. Jaque, G. Lifante, M. Aguiló, and F. Díaz, "Mirrorless buried waveguide laser in monoclinic double tungstates fabricated by a novel combination of ion milling and liquid phase epitaxy," Opt. Express **18**(26), 26937 (2010).
6. S. Aravazhi, D. Geskus, K. van Dalfsen, S. A. Vázquez-Córdova, C. Grivas, U. Griebner, S. M. García-Blanco, and M. Pollnau, "Engineering lattice matching, doping level, and optical properties of $KY(WO_4)_2$:Gd, Lu, Yb layers for a cladding-side-pumped channel waveguide laser," Appl. Phys. B: Lasers Opt. **111**(3), 433–446 (2013).
7. K. van Dalfsen, S. Aravazhi, C. Grivas, S. M. García-Blanco, and M. Pollnau, "Thulium channel waveguide laser with 16 W of output power and ~80% slope efficiency," Opt. Lett. **39**(15), 4380 (2014).
8. D. Geskus, S. Aravazhi, C. Grivas, K. Wörhoff, and M. Pollnau, "Microstructured $KY(WO_4)_2$:Gd^{3+}+, Lu^{3+}, Yb^{3+} channel waveguide laser," Opt. Express **18**(9), 8853 (2010).
9. D. Geskus, S. Aravazhi, K. Wörhoff, and M. Pollnau, "High-power, broadly tunable, and low-quantum-defect $KGd_{1-x}Lu_x(WO_4)_2$:Yb^{3+} channel waveguide lasers," Opt. Express **18**(25), 26107–26112 (2010).
10. F. Piantedosi, G. Y. Chen, T. M. Monro, and D. G. Lancaster, "Widely tunable, high slope efficiency waveguide lasers in a Yb-doped glass chip operating at 1 μm," Opt. Lett. **43**(8), 1902 (2018).
11. R. Mary, S. J. Beecher, G. Brown, R. R. Thomson, D. Jaque, S. Ohara, and A. K. Kar, "Compact, highly efficient ytterbium doped bismuthate glass waveguide laser," Opt. Lett. **37**(10), 1691 (2012).
12. Y. Tan, A. Rodenas, F. Chen, R. R. Thomson, A. K. Kar, D. Jaque, and Q. Lu, "70% slope efficiency from an ultrafast laser-written Nd:$GdVO_4$ channel waveguide laser," Opt. Express **18**(24), 24994 (2010).
13. T. Calmano, A.-G. Paschke, S. Müller, C. Kränkel, and G. Huber, "Curved Yb:YAG waveguide lasers, fabricated by femtosecond laser inscription," Opt. Express **21**(21), 25501 (2013).
14. J. Siebenmorgen, T. Calmano, K. Petermann, and G. Huber, "Highly efficient Yb:YAG channel waveguide laser written with a femtosecond-laser," Opt. Express **18**(15), 16035 (2010).
15. F. Chen and J. R. V. de Aldana, "Optical waveguides in crystalline dielectric materials produced by femtosecond-laser micromachining," Laser Photonics Rev. **8**(2), 251–275 (2014).
16. M. A. Sefunc, F. B. Segerink, and S. M. García-Blanco, "High index contrast passive potassium double tungstate waveguides," Opt. Mater. Express **8**(3), 629 (2018).

OSA CONTINUUM

17. P. A. Loiko, K. V. Yumashev, N. V. Kuleshov, G. E. Rachkovskaya, and A. A. Pavlyuk, "Detailed characterization of thermal expansion tensor in monoclinic $KRe(WO_4)_2$ (where Re = Gd, Y, Lu, Yb)," Opt. Mater. (Amsterdam, Neth.) **34**(1), 23–26 (2011).
18. SCHOTT, "MEMpax® Ultra-Thin Borosilicate Glass," http://www.schott.com/advanced_optics/english/products/optical-materials/thin-glass/mempax/index.html.
19. "ThermoFisher Scientific: Typical values of Microslides (Soda Lime Glass)," 8983 (n.d.).
20. Schott, "MICROCROWN Microscopy Glass," https://www.schott.com/advanced_optics/english/products/optical-materials/thin-glass/microscopy-glass-microcrown/index.html.
21. S. Keyvaninia, M. Muneeb, S. Stankovic, P. J. Van Veldhoven, D. Van Thourhout, and G. Roelkens, "Ultra-thin DVS-BCB adhesive bonding of III-V wafers, dies and multiple dies to a patterned silicon-on-insulator substrate," Opt. Mater. Express **3**(1), 35–46 (2013).
22. S. Stanković, R. Jones, J. Heck, M. Sysak, D. Van Thourhout, and G. Roelkens, "Die-to-Die Adhesive Bonding Procedure for Evanescently-Coupled Photonic Devices," Electrochem. Solid-State Lett. **14**(8), H326 (2011).
23. W. P. Maszara, G. Goetz, A. Caviglia, and J. B. McKitterick, "Bonding of silicon wafers for silicon-on-insulator," J. Appl. Phys. **64**(10), 4943–4950 (1988).
24. G. Kissinger and W. Kissinger, "Void-free silicon-wafer-bond strengthening in the 200–400 °C range," Sens. Actuators, A **36**(2), 149–156 (1993).
25. T. Allenet, D. Bucci, F. Geoffray, F. Canto, L. Couston, E. Jardinier, and J.-E. Broquin, "Packaged integrated opto-fluidic solution for harmful fluid analysis," in J.-E. Broquin and G. Nunzi Conti, eds. (International Society for Optics and Photonics, 2016), 9750, p. 975011.
26. Bohle, "UV-Klebstoff Verifix LV 740," 1–2 (n.d.).
27. NORLAND PRODUCTS INCORPORATED, "Norland Optical Adhesive 81," 1–2 (1966).
28. Epoxy Technology, "EPO-TEK 353ND," 1–2 (2014).
29. Epoxy Technology, "EPO-TEK 377," 1–2 (2015).
30. Dow Chemical Company, "CYCLOTENE ™ 3000 Series Advanced Electronics Resins," 1–10 (2012).
31. M. A. Sefunc, "New architectures for integrated optics: low-loss tight bends and on-chip high-index-contrast potassium double tungstate waveguides," University of Twente (2016).
32. S. Park, J. H. Park, S. Hwang, and J. Kwak, "Bench-top fabrication and electrochemical applications of a micro-gap electrode using a microbead spacer," Electrochem. Commun. **68**, 76–80 (2016).
33. C. I. van Emmerik, S. M. Martinussen, M. Dijkstra, S. M. García-Blanco, J. Mu, and R. Kooijman, "A novel polishing stop for accurate integration of potassium yttrium double tungstate on a silicon dioxide platform," Proc. SPIE **10535**, 105350U (2017).
34. U. Tong and Q.-Y. Gösele, *Semiconductor Wafer Bonding: Science and Technology* (John Willey & sons, inc, 1999).
35. K. Tanabe, K. Watanabe, and Y. Arakawa, "III-V/Si hybrid photonic devices by direct fusion bonding," Sci. Rep. **2**(1), 349 (2012).